

# Metasurface Loaded Two-Port Circularly Polarized Microstrip Array Antenna with High Gain Features for mm-wave 5G Communication System

Shashikant Verma, Ankit Pandit, Sanjeev Kumar Gupta

**Abstract** – This paper describes the design and analysis of 2-port aperture coupled printed radiator. Stair formed slot creates the circular polarization characteristics from 30.75-31.25 GHz. Mirror orientation of slot provides the support of LHCP with port-1 and RHCP with port-2. Due to which, the isolation level is found to be more than 30 dB. Array based structure is utilised to create broadsided radiation pattern with a gain of 5.0 dBi. For further enhancing the gain value, a double negative metamaterial made metasurface is suspended over the two-port radiator. It enhances the gain level to more than 11.0 dBi. Experimental results confirm the efficient working of designed aerial in between 30.25-31.75 GHz. Broadside far-field pattern and low correlation coefficient confirms its applicability for 5G communication system in mm-wave regime.

**Keywords** – Antenna Array, Antenna Gain, mm-wave, Circular Polarization

## I. INTRODUCTION

In the modern day, 5G technology has drawn a lot of interest because of its ability to provide fast data speeds and minimal latency [1]. Because increased data rates are closely correlated with bandwidth, research has placed a significant emphasis on mm-wave front ends. In 5G communication systems, two frequency bands are highly significant: sub-6 GHz band and mm-wave frequency band [2]. Mm-wave spectrum is wide famous because of its capability to provide wider bandwidth, which in turn provides high capacity. As the wavelengths go smaller, the mm-wave spectrum is particularly vulnerable to air attenuations, which can reduce the 5G experience [3]. The development of Multiple-Input Multiple-Output (MIMO) technology is crucial to address this problem. MIMO uses the multipath feature to increase channel limit and range efficacy without requiring an increase in information power [4]. In addition, the MIMO framework should transfer the characteristics of appropriate isolation between the elements and broadband to add a successful execution [5]. The increased mutual coupling between the MIMO antenna elements affects the MIMO antenna system's throughput [6].

Design a MIMO antenna and ensuring appropriate isolation between the components is an extremely challenging task. Different researchers have developed multiple techniques to

*Article history: Received July 30, 2024; Accepted December 20, 2024*

Shashikant Verma, Ankit Pandit and Sanjeev Kumar Gupta are with the Department of Electronics & Communication Engineering, Ravindranath Tagore University, Bhopal, India, Email: vermashashikant025@gmail.com, ankit.pandit@aiselectuniversity.ac.in, sanjeevkumar.gupta@aiselectuniversity.ac.in

design efficient MIMO radiator in mm-wave spectrum. In [7], a 4-element aerial configuration with a peak gain of 8.3 dB is proposed for a 5G communication system that spans the mm-wave frequency spectrum of 25.5-27.6 GHz. A SIW-fed aperture radiator is used in [8] to provide an array of multi-port radiator. This aerial for 5G covers the frequency ranges 27.5-28.35 GHz, with a maximum gain of 9.6 dB. For 5G applications, a multi-port aerial with a maximum gain of 9.5 dB and a frequency range of 26 to 29.5 GHz is suggested in [9]. A 5G metamaterial-based antenna with a peak gain value of 7.4 dB is shown in [10] for multi-port systems. A wideband multiport radiator having size 66.8x40x0.8 mm<sup>3</sup> with a frequency range of 2.6 to 13 GHz has been constructed [11]. In [12], a 4-element multi-port radiator covering the 5G spectrum in between 27.5-40 GHz with antenna size 158x77.8 mm<sup>2</sup> is presented.

This communication explains the design and analysis of two port printed radiator in mm-wave regime. Stair formed aperture coupling helps to get circular polarization features within the operating band. Array concept along with metasurface suspension helps to enhance the gain up to 11.0 dBi. Polarization diversity helps to improve the separation level by more than 25 dB. To understand the concept and verify the simulated outcome, this article is segmented as: (a) antenna layout; (b) antenna analysis; (c) experimental outcome; and (d) conclusion.

## II. ANTENNA LAYOUT AND OPTIMISED DIMENSION

The structural layout of proposed radiator is presented in Fig. 1. The two-port radiator is designed over the dual sandwiched RT Duroid substrate ( $\epsilon_r=2.2$ ) having thickness 0.254 mm. 3-dB power divider is utilised to make the array configuration. Microstrip line is placed on the lower port of the bottom substrate, while stair formed slot is placed on the upper side of bottom substrate. Top of sandwiched substrate contains microstrip radiator, which is electromagnetically coupled with slot present on the bottom substrate. Metasurface is also made on the RT Duroid substrate. Table 1 lists the optimised dimension of different antenna parameters.

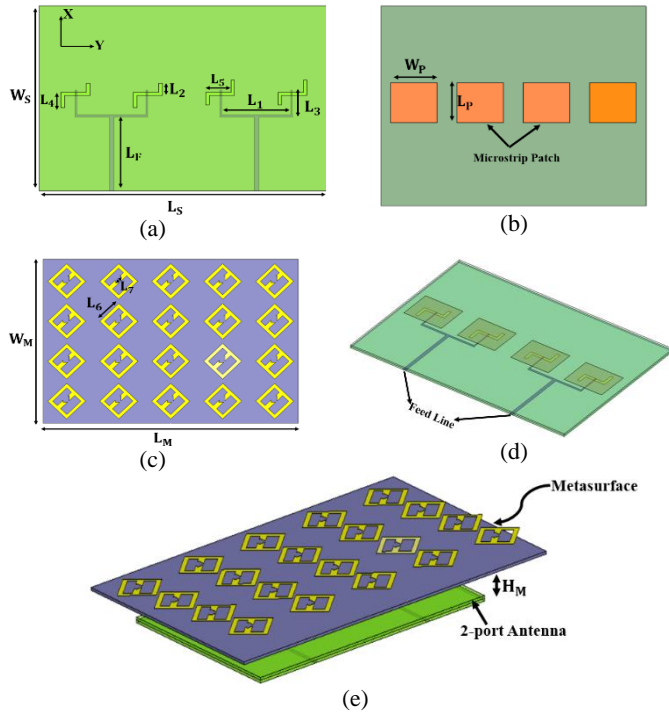


Fig. 1. Antenna Layout: (a) Feed Design, (b) 2-port radiator, (c) Metasurface, (c) 3D view of Radiator, (d) 3D view of Proposed Design

TABLE 1  
OPTIMAL SIZE OF VARIOUS RADIATOR PARAMETER

Symbol	Dimension (mm)	Symbol	Dimension (mm)
$L_S$	40.0	$W_S$	30.0
$L_M$	54.0	$W_M$	37.0
$H_M$	3.0	$W_P$	7.0
$L_P$	6.0	$L_F$	12.0
$L_1$	10.0	$L_2$	1.5
$L_3$	4.0	$L_4$	2.0
$L_5$	4.0	$L_6$	4.0
$L_7$	1.0	$W_S$	0.5

### III. ANTENNA ANALYSIS

This section focuses on the detailed examination of designed radiator and it has been carried out using HFSS EM simulator. For better understanding, this section is divided into two subsegments i.e. A. single port investigation; and B. dual port investigation.

#### A. Single Port Investigation

Figure 2 presents the reflection coefficient analysis of single port antenna with modification in slot shape. Four different cases are taken: (a) horizontal slot coupled patch without array configuration; (b) stair slot with equal arm length coupled patch without array configuration; (c) stair slot with unequal arm length coupled patch without array configuration; and (d) stair slot with unequal arm length coupled patch with array configuration. From Fig. 2, it is confirmed that normal patch is resonating at 31.35 GHz.

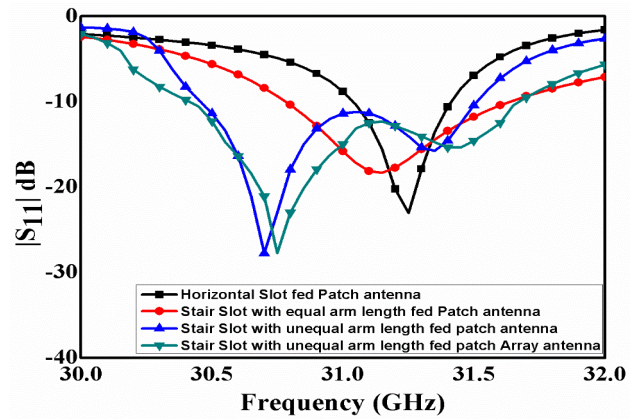


Fig. 2.  $|S_{11}|$  variation with different changes in the shape slot

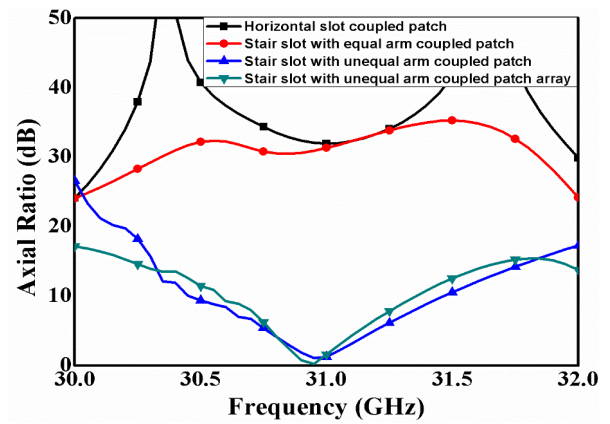


Fig. 3. Axial Ratio variation with different changes in the shape slot

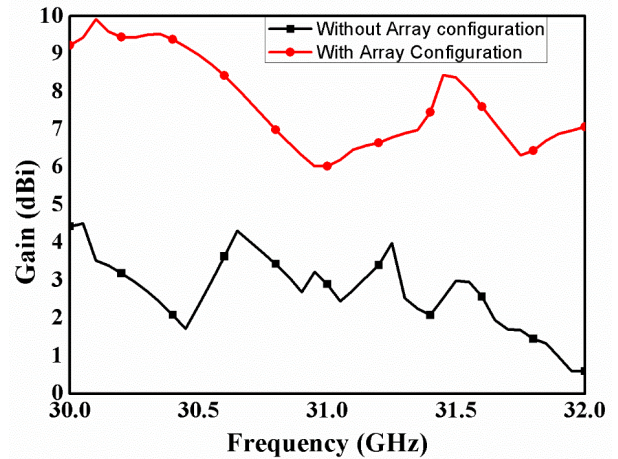


Fig. 4. Gain variation with and without array configuration

Stair shaped with unequal arm length creates dual resonating peaks due to generation of orthogonal modes. Conversion of array configuration also have same reflection coefficient features. Fig. 3 shows the axial ratio variation for all the aforementioned cases. It can be seen from Fig. 3 that axial ratio comes down to 3-dB in case of stair formed slot with unequal arm length coupled patch. Stair shaped slot coupling produces the orthogonal field lines inside the patch, while unequal arm length produces the 90° phase shift between the field lines [13]. In this way, both the conditions circular

polarization is fulfilled and CP waves are created in between 30.8-31.2 GHz. Array configuration also possess the same axial ratio as normal patch radiator in single port configuration.

Figure 4 presents the gain variation with and without array configuration towards broadsided direction. It is seen from Fig. 4 that array configuration improves the gain around 8.0 dBi. It is due to Array configuration adds the far-field obtained from different radiating element constructively, which in turn enhance the directivity/gain of antenna.

### B. Dual Port Investigation

Now, the single port antenna is converted into the dual port configuration with two different cases: (i) stair aperture having unequal arm length with same slot orientation; and (ii) stair aperture having unequal arm length with mirror slot orientation. Figure 5 shows the S-parameter variation for single port and dual port having both configurations. It can be seen from Fig. 5 that reflection coefficient is approx. same for all cases and isolation is better (more than 25 dB) in case of mirror aperture orientation.

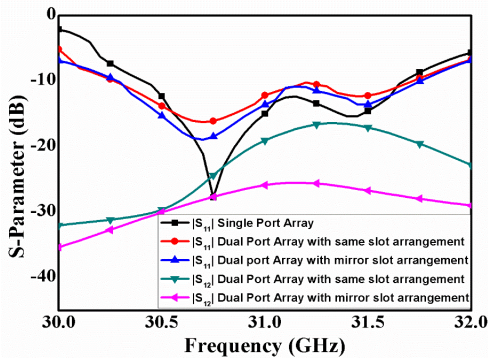


Fig. 5. S-parameter variation with single and dual port Antenna

In order to make metasurface, a unit cell is designed and its effective permittivity and permeability is shown in Fig. 6. It has been extracted by using following formula [14]:

$$Z = \pm \left[ \frac{(1+S_{11})^2 - S_{21}^2}{(1-S_{11})^2 - S_{21}^2} \right]^{0.5} \quad (1)$$

$$e^{jn_0d} = \frac{S_{21}}{1-S_{11} \frac{Z-1}{Z+1}} \quad (2)$$

$$\epsilon = \frac{\eta}{Z} \quad (3)$$

$$\mu = Z * \eta \quad (4)$$

In the above equations, ‘ $\mu$ ’, ‘ $\eta$ ’ and ‘ $z$ ’ indicate the permeability, intrinsic impedance and input impedance of unit cell. It is seen from Fig. 6 that the effective permittivity and permeability are negative with in the working spectrum. It means the designed unit cell acts as double negative (DNG) material.

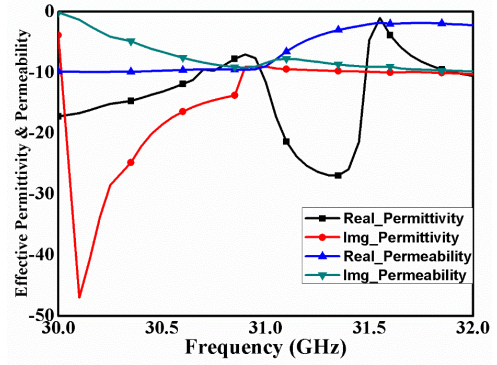


Fig. 6. Permittivity and Permeability change over frequency of designed unit cell

Now, the unit cell is arranged periodically to make the metasurface and suspended over the twin port radiator. Figure 7 presents the S-parameter variation in presence and absence of metasurface (MS). It can be observed from Fig.7 that S-parameter variation i.e. reflection coefficient and mutual coupling is not much effected by placing the MS. Fig. 8 shows the axial ratio variation with single port array and dual port with MS. From Fig. 8, it is confirmed that CP bandwidth is approx. same in both cases. Figure 9 shows the gain variation with and without MS towards broadside direction. It is perceived from Fig. 9 that the value is gain is approximately increased by 3.0 dBi within the working band. The maximum value of gain is around 11.5 dBi within the working spectrum. Double negative metasurface improves the directivity of the radiator [16].

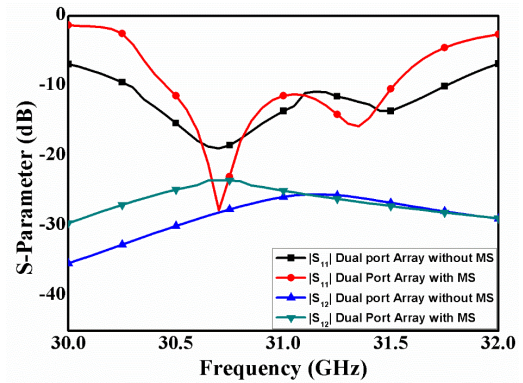


Fig. 7. S-parameter alteration with and without Metasurface (MS)

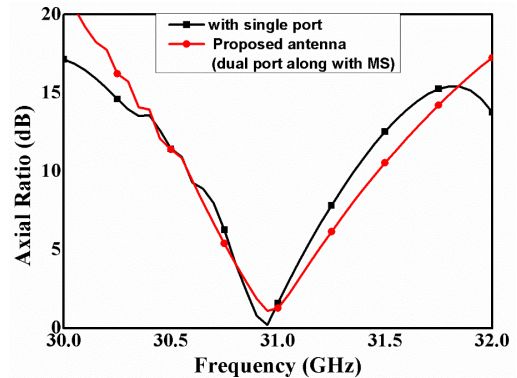


Fig. 8. Axial Ratio alteration with single port and dual port (with MS) radiator

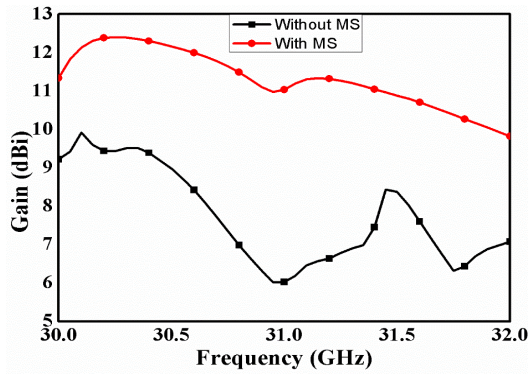


Fig. 9. Gain alteration with and without metasurface (MS)

#### IV. EXPERIMENTAL OUTCOME

The present part presents an assessment between the experimenting and computerized outcomes for the designed aerial. Figure 10 shows the pictures of antenna prototype. It is fabricated using chemical etching process on the RT Duroid substrate. Its S-parameter is measured using Agilent N524A PNA and far-field parameters are measured within the anechoic chamber. Figure 11 presents the comparison of measured and simulated S-parameter of proposed aerial. It can be seen from Fig. 11 that measured Scattering parameter is well matched with simulated one. The proposed antenna works effectively in between 30.25-31.75 GHz. Figure 12 shows the measured and simulated axial ratio variation for proposed design. Axial ratio measured within the anechoic chamber and used the concept of dual linear pattern technique [13]. It can be seen from Fig. 12 that there is good treaty between measured and simulated axial ratio. The proposed antenna design supports CP waves 30.75-31.25 GHz.

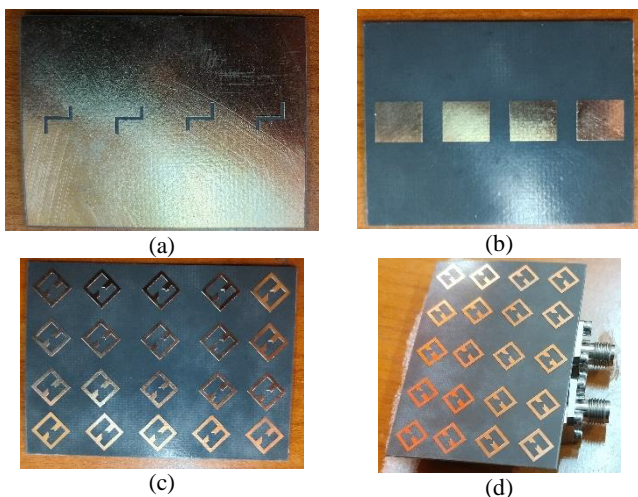


Fig. 10. Pictures of Fabricated Antennas: (a) Top View, (b) bottom View, (c) Metasurface, (d) Proposed Antenna

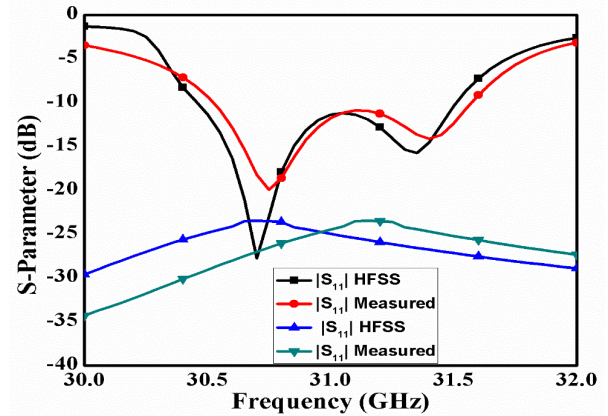


Fig. 11. Measured and Simulated S-parameter of Proposed Antenna Design

Figure 13 presents the measured/simulated LHCP and RHCP patterns in XZ plane with port-1 at 31.0 GHz. There is good treaty between measured and simulated pattern.

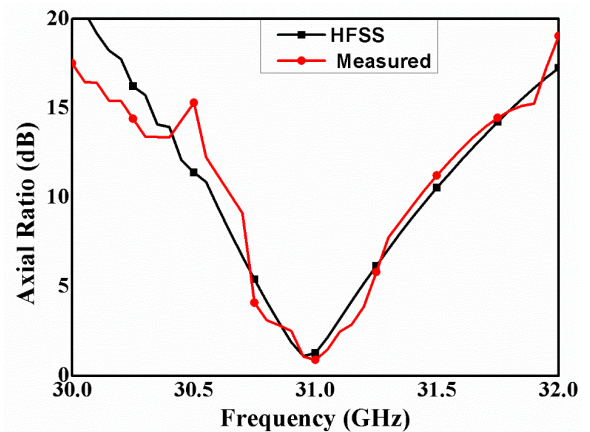


Fig. 12. Measured and Simulated Axial Ratio of Proposed Antenna Design

Two important observations are found: (i) LHCP is dominant port-1 and RHCP is dominant in case of port-2, which means the designed aerial supports the polarization diversity concept; and (ii) directive pattern is obtained with both the ports. Figure 14 presents the measured and simulated gain variation. It is measured using two antenna technique [13]. It is seen from Fig. 14 that there is good correlation between measured and simulated gain. The maximum value of gain within the working spectrum is around 11.8 dBi. Table 2 lists the performance of designed mm-wave radiator with other existing mm-wave MIMO antennas on the basis of size, gain, bandwidth and isolation. It can be observed from Table 2 that overall performance of designed radiator is better as compare to published mm-wave antenna. Circular polarization provides the additional features to proposed radiator.

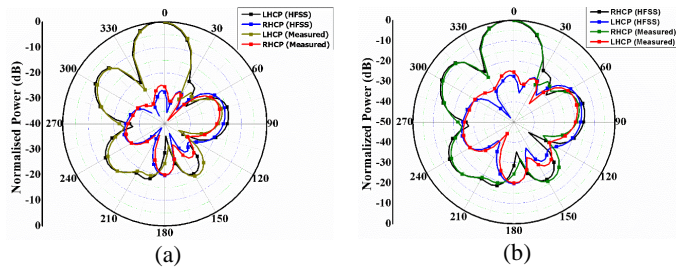


Fig. 13. Measured and Simulated LHCP/RHCP pattern in XZ plane at 31.0 GHz: (a) Port-1, (b) Port-2

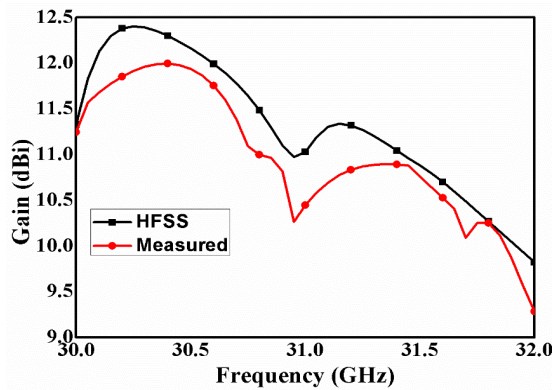


Fig. 14. Measured/Simulated Gain variation for proposed radiator

TABLE 2

COMPARATIVE ASSESSMENT OF DESIGNED RADIATOR WITH EXISTING MM-WAVE RADIATORS ON THE ANTENNA SIZE, GAIN AND AXIAL RATIO AND IMPEDANCE BANDWIDTH

Ref	Antenna Size (mm <sup>2</sup> )	Working Bandwid. (GHz)	AR Bandwid. (GHz)	Max. Gain (dBi)	Isolation
[7]	40x45	2.1	NA	8.5	>20 dB
[8]	45x48	0.85	NA	9.6	>20 dB
[9]	39x39	2.5	NA	8.9	>20 dB
[10]	30x30.5	1.5	NA	7.4	>15 dB
[11]	66.8x40	1.75	NA	6.0	>15 dB
[12]	158x77.8	1.5	NA	6.0	>17 dB
Proposed	40x30	1.75	0.5	11.8	>25 dB

Finally, to check the efficiency of designed aerial in terms of diversity parameters, envelop correlation coefficient (ECC) and diversity gain (DG) comes into the picture. ECC confirms the similarity contents among the antenna ports. Lower value of ECC (less than 0.2) shows the better working of MIMO

antenna [16]. DG shows the overall gain of MIMO antenna in fading environment. Its standard value lies approx. 10 dB for efficient radiator [16]. Figure 14 shows the ECC and DG variation for proposed antenna. It is clearly visible from Fig. 14 that the value of DG is around 10 dB, while ECC is well below to 0.2 within the working spectrum for proposed antenna.

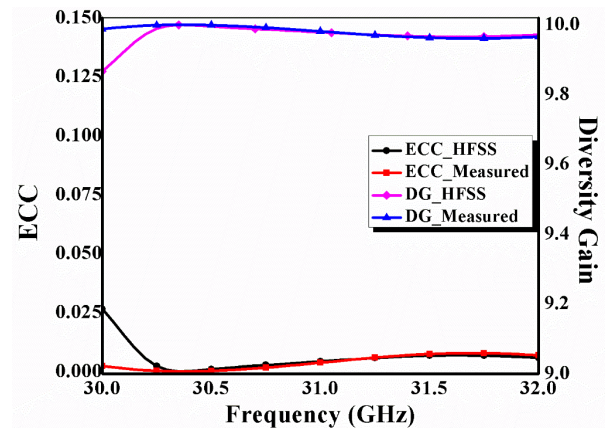


Fig. 14 Measured/Simulated ECC and DG variation of proposed antenna

## V. CONCLUSION

This communication has explained the design and investigation of two port microstrip array radiator. It works effectively in between 31.5-33.25 GHz. The unique features of designed aerial are: (i) high value of gain (more than 11.0 dBi) due to combination of array antenna concept and suspension of DNG metasurface; (ii) stair formed slot provides the CP waves within the working spectrum i.e. 32.05-32.68 GHz; and (iii) mirror placement of feed improves the separation level by more than 30 dB. Low value of ECC and directive far-field features make the radiator effective for 5G communication system in mm-wave regime.

## REFERENCES

- [1] J. Zhang, X. Yu and K. B. Letaief, "Hybrid Beam Forming for 5G and Beyond Millimeter-Wave Systems: A Holistic View", *IEEE Open Journal of the Communications Society*, vol. 1, pp. 77-91, 2019, DOI: 10.1109/OJCOMS.2019.2959595
- [2] R. Przesmycki, M. Bugaj and L. Nowosielski, "Broadband Microstrip Antenna for 5G Wireless Systems Operating at 28 GHz", *Electronics*, vol. 10, p. 1, 2021, DOI:10.3390/electronics10010001
- [3] M. B. Almashhdany, A. A. Oras, M. S. Ahmed, A. Mohamed, H. Naba and A. Fatima, "Design of Multi-Band Slotted Mmwave Antenna for 5G Mobile Applications", *Proceedings of the IOP Conference Series: Materials Science and Engineering*, vol. 881, no. 1, April 2020, DOI: 10.1088/1757-899X/881/1/012150
- [4] L. Sun, Y. Li, Z. Zhang and Z. Feng, "Wideband 5G MIMO Antenna with Integrated Orthogonal-Mode Dual-Antenna Pairs for Metal-Rimmed Smartphones", *IEEE Transaction Antennas and Propagation*, vol. 68, pp. 2494-2503, 2020, DOI: 10.1109/TAP.2019.2948707

- [5] M. Abdullah, S. H. Kiani and A. Iqbal, "Eight Element Multiple-Input Multiple-Output (MIMO) Antenna for 5G Mobile Applications", *IEEE Access*, vol. 7, pp. 134488-134495, 2019, DOI: 10.1109/ACCESS.2019.2941908
- [6] X. Yuan, W. He, K. Hong, C. Han, Z. Chen and T. Yuan, "Ultra-Wideband MIMO Antenna System With High Element-Isolation for 5G Smartphone Application", *IEEE Access*, vol. 8, pp. 56281-56289, 2020, DOI: 10.1109/ACCESS.2020.2982036
- [7] M. Khalid, S. I. Naqvi, N. Hussain, M. Rahman, S. S. Mirjavadi, M. J. Khan, and Y. Amin, "4 Port MIMO Antenna with Defected Ground Structure for 5G Millimeter Wave Applications", *Electronics*, vol. 9, no. 71, 2020, DOI: 10.3390/electronics9010071
- [8] B. Yang, Z. Yu, Y. Dong, J. Zhou and W. Hong, "Compact Tapered Slot Antenna Array for 5G Millimeter-Wave Massive MIMO Systems", *IEEE Transaction Antennas and Propagation*, vol. 65, pp. 6721-6727, 2017, DOI: 10.1109/TAP.2017.2700891
- [9] N. Hussain, M. Jeong, J. Park and N. Kim, "A Broadband Circularly Polarized Fabry-Perot Resonant Antenna Using a Single-Layered PRS for 5G MIMO Applications", *IEEE Access*, vol. 7, pp. 42897-42907, 2019, DOI: 10.1109/ACCESS.2019.2908441
- [10] H. Jiang, L. Si, W. Hu and X. Lv, "A Symmetrical Dual-Beam Bowtie Antenna With Gain Enhancement Using Metamaterial for 5G MIMO Applications", *IEEE Photonics Journal*, vol. 11, pp. 1-9, 2019, DOI: 10.1109/JPHOT.2019.2891003
- [11] S. R. Patre and S. P. Singh, "Broadband Multiple-Input Multiple-Output Antenna Using Castor Leaf-Shaped Quasi-Self-Complementary Elements", *IET Microwaves, Antennas and Propagation*, vol. 10, 1673-1681, IET, 2016, DOI: 10.1049/iet-map.2016.0058
- [12] E. A. Abbas, M. Ikram, A. T. Mobashsherband and A. Abbosh, "MIMO Antenna System for Multi-Band Millimeter-Wave 5G and Wideband 4G Mobile Communications", *IEEE Access*, vol. 7, pp. 181916-181923, 2019, DOI: 10.1109/ACCESS.2019.2958897
- [13] C. A. Balanis, *Antenna Theory: Analysis and Design*, John Wiley & Sons, 2016
- [14] M. S. Sharawi and A. B. Numan, "Extraction of Material Parameters for Metamaterials Using A Full-Wave Simulator [education column]", *IEEE Antennas and Propagation Magazine*, vol. 55, no. 5, pp. 202-211, 2013, DOI: 10.1109/MAP.2013.6735515
- [15] D. Samantaray and S. Bhattacharyya, "A Gain-Enhanced Slotted Patch Antenna Using Metasurface as Superstrate Configuration", *IEEE Transactions on Antennas and Propagation*, vol. 68, no. 9, pp. 6548-6556, 2020, DOI: 10.1109/TAP.2020.2990280
- [16] M. S. Sharawi, *Printed MIMO Antenna Engineering*, Norwood, MA, USA, Artech House, 2014